

Rotational and magnetic instability in the diffusive tachocline

BASHIR W. SHARIF and CHRIS A. JONES*

Department of Mathematical Sciences, University of Exeter, EX4 4QE, UK

(Received 1 August 2005; In final form 16 September 2005)

In this paper we study the linear instability of the two-dimensional strongly stratified model for global MHD in the diffusive solar tachocline. Gilman and Fox (1997) showed that for ideal MHD, the observed surface differential rotation becomes more unstable than is predicted by Watson's (1981) nonmagnetic analysis. They showed that the solar differential rotation is unstable for essentially all reasonable values of the differential rotation in the presence of an antisymmetric toroidal field. They found that for the broad field case $B_\phi \sim \sin \theta \cos \theta$, θ being the co-latitude, instability occurs only for the azimuthal $m = 1$ mode, and concluded that modes which are symmetric (meridional flow in the same direction) about the equator onset at lower field strengths than the antisymmetric modes. We study the effect of viscosity and magnetic diffusivity in the strongly stably stratified case where diffusion is primarily along the level surfaces. We show that antisymmetric modes are now strongly preferred over symmetric modes, and that diffusion can sometimes be destabilising. Even solid body rotation can be destabilised through the action of magnetic field. In addition, we show that when diffusion is present, instability can occur when the longitudinal wavenumber $m = 2$.

Keywords: Solar tachocline; Instabilities; Differential rotation; Magnetic field

1. Introduction

Helioseismic observations show that there is a shear layer confined between the convection zone and the radiative zone of the Sun (see, for example, Schou *et al.* 1998, Charbonneau *et al.* 1999). The existence of this layer is related to the transition from differential rotation in the convection zone to almost solid (uniform) rotation in the radiative zone. Spiegel and Zahn (1992) called this layer the solar tachocline and it is thought to be of crucial importance in the origin of solar activity phenomena. The thickness, h , of this transition region is estimated to be $h \approx 0.05r_\odot$ where r_\odot is the solar radius, (Brown *et al.* 1989, Kosovichev 1996), though its exact width is still controversial.

Because of the strongly stable stratification in the radiative zone, radial motion is heavily suppressed (Spiegel and Zahn 1992), but the horizontal shear may drive motion in nearly parallel two-dimensional spherical shells. Prior to the discovery of the tachocline, Watson (1981) considered the linear stability of a differentially rotating flow with angular velocity $\Omega = \Omega_0(1 - s_2 \cos^2 \theta)$, where θ is the co-latitude, taken to model the solar differential rotation. He found that the flow is unstable to two-dimensional disturbances on the spherical surfaces provided $s_2 > 2/7 = 0.286$. This critical value of s_2 is similar to the solar value. However, Charbonneau *et al.* (1999) noted that if the differential rotation profile is taken as $\Omega = \Omega_0(1 - s_2 \cos^2 \theta - s_4 \cos^4 \theta)$, the critical value of s_2 is very sensitive to even small values of s_4 , so the instability is dependent on the exact form of the differential rotation in the tachocline.

Gilman and Fox (1997), henceforward referred to as GF97, extended Watson's analysis to the case with an imposed, equatorially antisymmetric, azimuthal magnetic field. They found that magnetic fields of a strength which may plausibly exist in the tachocline region can also significantly reduce the value of s_2 needed for instability. They concluded that with a magnetic field the solar differential rotation in the tachocline was likely to be unstable. These instabilities may play a role in the solar

*Corresponding author. Present address: Department of Applied Mathematics, University of Leeds, Leeds, LS2 9JT, UK. E-mail: C.A.Jones@maths.leeds.ac.uk

dynamo, they may also limit the field strength in the tachocline, and they may redistribute angular momentum in the tachocline, possibly accounting for why the tachocline is thin. Most previous work has considered only two-dimensional disturbances, and it is an open question whether three-dimensional disturbances could play an important role, (Cally 2003).

Dikpati *et al.* (2004) recently considered the effect of radial diffusion on the stability of a magnetic differentially rotating tachocline and showed that it provides a drag term in the equations. They found that diffusion generally increased the stability of the system, and could if strong enough eliminate instability altogether. They also noted that magnetic diffusion was more important than viscous diffusion in promoting stability.

Diffusion in a system as large as the tachocline must be an eddy diffusion, due to small-scale motions transporting momentum and magnetic field. The strong suppression of radial motion on all horizontal length scales due to the strong stable stratification makes it likely that eddy transport will be primarily in the horizontal direction, so that even though the tachocline is thin, a horizontal eddy diffusivity may be a more plausible form of diffusion than the simple drag due to radial friction considered by Dikpati *et al.* (2004). There is the possibility, though, that magnetic fields or gravity wave propagation could couple adjacent shells together, however, and our simple two-dimensional model ignores such coupling. A simple scale analysis, (Sharif 2005), suggests that the ratio of vertical to horizontal velocities in the tachocline is of order $(L/D)(\Omega/N)^2$, where L is the horizontal length-scale of the motion, D the tachocline thickness, Ω is the solar rotation rate and N is the Brunt-Väisälä frequency. Even though the tachocline is thin, $D/L \ll 1$, vertical velocities are very small compared to horizontal velocities because the period of gravity waves in the tachocline is of the order of a few hours or less, very short compared to the differential rotation timescale. In the very thin convective overshoot region just below the convection zone, N is much smaller, and vertical velocities there will be comparable to horizontal velocities.

The interior angular velocity, Ω_i , lies between the angular velocities at the equator, Ω_e , and at the poles, Ω_p , in the convection zone. The sharp change of the angular velocity was estimated to be near $r_0 = 0.7r_\odot$. It has important consequences for the generation of the solar magnetic field and its reversal process during the 22-year magnetic cycle, (Durney 2000, Forgács and Petrovay 2001). It is also believed that the non-uniform rotation makes a shear that deforms magnetic lines of force originally spread in meridional planes and hence builds up the strong toroidal field that is necessary for the formation of sunspots. Moreover, the centre of upwelling should be at a latitude of about 30 degrees (where, incidentally, sunspots emerge at the start of a new cycle). This process is one of the essential ingredients of $\alpha\Omega$ dynamos, (e.g. Roberts and Soward 1992, Charbonneau and MacGregor 1997, Zhang *et al.* 2003, Chan *et al.* 2004).

2. Physical assumptions and governing equations

The instability that we discuss here is related to that of GF97, except that our analysis contains the kinematic viscosity ν and magnetic diffusivity λ factors while theirs does not. The flow will be assumed to be on a two-dimensional spherical shell with radial variation ignored, following the assumption that diffusive processes are highly anisotropic, as discussed in section 1. The fluid under investigation is considered to be incompressible, with constant density ρ , electrically conducting and viscous. We neglect any conductive or internal heating and assume adiabatic flow, and we also assume the fluid is Boussinesq, justified because of the thinness of the tachocline. Additionally, we assume the solar differential rotation is maintained by convection in the solar convection zone and this gives rise to a body force $F\hat{\phi}$ in the azimuthal direction which maintains the reference state differential rotation against viscosity. Similarly, the basic state azimuthal magnetic field is generated by a dynamo process which maintains it against magnetic diffusion.

We use spherical polar coordinates, r , θ , and ϕ , which are the distance from the Sun's centre, the co-latitude, and the longitude respectively. The velocities in the eastward ($\hat{\phi}$ -direction) and

southward ($\hat{\boldsymbol{\theta}}$ -direction) are u and v respectively. To describe the dynamical motion of our system, based on these assumptions, we use the Navier-Stokes equation in an inertial frame of reference and the induction equation,

$$\rho \left(\frac{\partial \mathbf{u}}{\partial t} + \mathbf{u} \cdot \nabla \mathbf{u} \right) = -\nabla p + \rho \nu \nabla^2 \mathbf{u} + \frac{1}{\mu_o} (\nabla \times \mathbf{B}) \times \mathbf{B} + F \hat{\boldsymbol{\phi}}, \quad (1)$$

$$\frac{\partial \mathbf{B}}{\partial t} = \nabla \times (\mathbf{u} \times \mathbf{B}) + \lambda \nabla^2 \mathbf{B}, \quad (2)$$

$$\nabla \cdot \mathbf{u} = \mathbf{0}, \quad \nabla \cdot \mathbf{B} = \mathbf{0}. \quad (3)$$

The reference state about which we perturb the system is

$$\bar{\mathbf{u}} = \Omega_0 (1 - s_2 \cos^2 \theta) r_0 \sin \theta \hat{\boldsymbol{\phi}}, \quad \bar{\mathbf{B}} = B_0 \cos \theta \sin \theta \hat{\boldsymbol{\phi}}, \quad (4)$$

together with a basic state pressure \bar{p} . We have not included the dynamo forcing term in equation (2) which would be required to maintain this reference state field against diffusion, but we are tacitly assuming that this forcing takes no part in the development of any instability. The form of \mathbf{B} is chosen to make it antisymmetric about the equator, as observed for the solar toroidal field, and the $\sin \theta$ factor ensures that the toroidal field goes to zero at the poles, again a reasonable assumption since the bulk of the solar toroidal field occurs in mid-latitudes. Note that the reference state is independent of longitude, ϕ . This state can be perturbed by setting

$$p = \bar{p} + p', \quad \mathbf{u} = \bar{\mathbf{u}} + \mathbf{u}', \quad \text{and} \quad \mathbf{B} = \bar{\mathbf{B}} + \mathbf{B}' \quad (5)$$

and letting

$$\mathbf{u}' = u \hat{\boldsymbol{\phi}} + v \hat{\boldsymbol{\theta}}, \quad \mathbf{B}' = a' \hat{\boldsymbol{\phi}} + b' \hat{\boldsymbol{\theta}}, \quad (6)$$

where an overbar and the primes denote the reference state and perturbations respectively. Since the flow and field remain two-dimensional, from (3) we can write

$$u = -\frac{1}{r_0} \frac{\partial \psi}{\partial \theta}, \quad v = \frac{1}{r_0 \sin \theta} \frac{\partial \psi}{\partial \phi}, \quad a' = -\frac{1}{r_0} \frac{\partial \chi}{\partial \theta}, \quad b' = \frac{1}{r_0 \sin \theta} \frac{\partial \chi}{\partial \phi}, \quad (7)$$

so that ψ is the streamfunction for the flow, and χ the equivalent variable for the magnetic field. We non-dimensionalise the equations with respect to a unit of time $1/\Omega_0$, a unit of length r_0 and a unit of magnetic field $r_0 \Omega_0 \sqrt{\mu_o \rho}$. Since our equations are linear, and our basic state is independent of time and ϕ , we can write

$$\psi(\phi, \theta, t) = \tilde{\psi}(\theta) e^{im(\phi - \omega t)}, \quad \chi(\phi, \theta, t) = \tilde{\chi}(\theta) e^{im(\phi - \omega t)}. \quad (8)$$

We take the radial component of the curl of equation (1), and the induction equation (2), to obtain the governing pair of ordinary differential equations in the variable $\mu = \cos \theta$ in dimensionless form

$$(\Omega - \omega) \mathcal{L}(\tilde{\psi}) - \tilde{\psi} \frac{d^2}{d\mu^2} [\Omega(1 - \mu^2)] - a\mu \mathcal{L}(\tilde{\chi}) + a\tilde{\chi} \frac{d^2}{d\mu^2} [\mu(1 - \mu^2)] = (imR_e)^{-1} \mathcal{L}^2(\tilde{\psi}) \quad (9)$$

and

$$a\mu \tilde{\psi} = (\Omega - \omega) \tilde{\chi} + (imR_m)^{-1} \mathcal{L}(\tilde{\chi}). \quad (10)$$

where

$$\mathcal{L} \equiv \frac{d}{d\mu} (1 - \mu^2) \frac{d}{d\mu} - \frac{m^2}{1 - \mu^2}, \quad \Omega = 1 - s_2 \mu^2. \quad (11)$$

\mathcal{L} is the associated Legendre operator. The dimensionless parameters appearing in (9) and (10) are

$$R_e = \frac{\Omega_0 r_0^2}{\nu}, \quad R_m = \frac{\Omega_0 r_0^2}{\lambda}, \quad a = \frac{B_0}{\Omega_0 r_0 \sqrt{\mu_o \rho}}. \quad (12)$$

R_e is the fluid Reynolds number and R_m is the magnetic Reynolds number for our problem. Taking $\Omega_0 = 2.8 \times 10^{-6} \text{ s}^{-1}$, $r_0 = 5 \times 10^8 \text{ m}$, and $\nu \sim \lambda \approx 10^9 \text{ m}^2 \text{ s}^{-1}$ (Rüdiger 1989), then $R_e \approx R_m \approx 700$.

The value of the diffusion coefficients is of course very poorly known. If it is smaller than this estimate, then of course the corresponding Reynolds numbers will be larger. The parameter a measures the strength of the magnetic field. Since $\Omega_0 r_0$ is the fluid velocity due to the solar rotation at the equator, and $B_0/\sqrt{\mu_0 \rho}$ is the Alfvén speed, a is the reciprocal of the Alfvén Mach number. Taking the density at the base of the convection zone as $\rho \approx 0.19 \times 10^3 \text{ kg m}^{-3}$ (Guenther et al. 1992), $a = 1$ corresponds to a value of B_0 of about 22T or 220,000G, which makes the typical field in our model around 100kG. The diffusion terms in (9) and (10) only involve the horizontal derivatives through the operator \mathcal{L} . This is a consequence of our assumption that diffusive processes in the horizontal direction dominate over those in the radial direction, the opposite limit to that considered by Dikpati *et al.* (2004). Note that if the fluid and magnetic Reynolds numbers, R_e and R_m are very large, then we reach the ideal MHD case and the system of equations will be similar to that of GF97.

As in the non-magnetic case, both the momentum equation and induction equation are singular at $\mu = \pm 1$, so there are solutions which are finite and solutions which tend to infinity as $\mu \rightarrow \pm 1$. Therefore, the boundary conditions are that the singular solutions must be rejected, so

$$\tilde{\psi}(\mu) \quad \text{and} \quad \tilde{\chi}(\mu) \quad \text{must be finite at} \quad \mu = \pm 1. \quad (13)$$

For the flow and the magnetic field to be finite near the poles, we must have

$$\psi(\tilde{\mu}) = 0 \quad \text{and} \quad \tilde{\chi}(\mu) = 0 \quad \text{at} \quad \mu = \pm 1. \quad (14)$$

3. Method of solution

Following Watson (1981), the numerical solution of equations (9) and (10) can be achieved by expanding $\tilde{\psi}$ and $\tilde{\chi}$ as a series of associated Legendre polynomials for each longitudinal wavenumber m in the form of

$$\tilde{\psi}(\mu) = \sum_{n=m}^N a_n P_n^m(\mu) \quad \text{and} \quad \tilde{\chi}(\mu) = \sum_{n=m}^N b_n P_n^m(\mu), \quad (15)$$

where a_n and b_n are the coefficients of the series, and N is a truncation parameter, using the fact that

$$\mathcal{L}P_n^m = -n(n+1)P_n^m.$$

We get from (9)

$$\begin{aligned} -(\Omega - \omega) \sum_{n=m}^N n(n+1)a_n P_n^m - \frac{d^2}{d\mu^2} [\Omega(1 - \mu^2)] \sum_{n=m}^N a_n P_n^m + a\mu \sum_{n=m}^N n(n+1)b_n P_n^m \\ + \frac{d^2}{d\mu^2} [a\mu(1 - \mu^2)] \sum_{n=m}^N b_n P_n^m = \sum_{n=m}^N (imR_e)^{-1} n^2(n+1)^2 a_n P_n^m \end{aligned} \quad (16)$$

and

$$a\mu \sum_{n=m}^N a_n P_n^m = (\Omega - \omega) \sum_{n=m}^N b_n P_n^m - \sum_{n=m}^N (imR_m)^{-1} n(n+1)b_n P_n^m \quad (17)$$

from (10). We now use the recurrence relations (see Appendix A), together with $\Omega = 1 - s_2 \mu^2$, to transform (16) and (17) into a set of matrix equations for the coefficients a_n and b_n . These matrix equations form a linear matrix eigenvalue problem for ω . The matrices can be divided into a block structure (see Appendix A for details). The truncation parameter N was determined by increasing N until convergence was obtained. For some parameter values this required N to be up to around 500. Our matrices have the same structure as those used by GF97, but the diffusion terms change the actual matrices themselves (see appendix A for details of the coefficients). The

matrix eigenvalue problem was solved using standard NAG software routines. The eigenvalue ω is determined along with the coefficients in the expansions (15), so that the eigenfunctions can be reconstructed from the eigenvectors of the matrix eigenvalue problem. We can have disturbances which are either symmetric or antisymmetric about the equator. We use the same notation for these symmetries as GF97 did, that is the symmetric disturbances are denoted by $(\tilde{\psi}_s, \tilde{\chi}_a)$ and the antisymmetric disturbances by $(\tilde{\psi}_a, \tilde{\chi}_s)$. Symmetric disturbances therefore have only non-zero coefficients a_{m+2k}, b_{m+2k+1} for integer $k \geq 0$, and antisymmetric disturbances only have non-zero coefficients a_{m+2k+1}, b_{m+2k} .

4. Results of the stability analysis

Recall that the growth rates, $m\omega_i$, for various values of s_2 , are scaled by the equatorial rotation rate. A growth rate of 0.01 is equivalent to an e -folding growth time of about 12 months on the Sun, so that, for example, $\omega_i=0.001$ is equivalent to about a 10 year growth rate. A value of $s_2 = 0.30$ is approximately the photospheric differential rotation rate. In addition when we include the Reynolds numbers, (R_e and R_m), in our calculations, we keep the ratio of R_m to R_e to be unity. The usual argument is that the diffusion is due to turbulent eddies, and $\lambda \approx \nu \approx u_T \cdot l$ where u_T is the magnitude of the turbulent velocity and l is a typical length scale of the turbulent eddies. So it is sensible to take $P_m = \nu/\lambda = 1$, though there is no very rigorous argument indicating this is correct. This ratio is called the magnetic Prandtl number, P_m . Recall also that a dimensionless toroidal magnetic field parameter $a = 1$ corresponds to peak toroidal magnetic fields of about 2.2×10^5 G below the solar convection zone.

In the presence of toroidal magnetic field with no diffusion, GF97 found a new set of instabilities with the differential rotation lower than the conventional value, $s_2 = 0.30$. They showed that the instabilities for $m = 1$ that are symmetric $(\tilde{\psi}_s, \tilde{\chi}_a)$ about the equator dominate when the toroidal field strength $a \leq 0.3$ but as the parameter a gets larger the antisymmetric $(\tilde{\psi}_a, \tilde{\chi}_s)$ modes become more dominant. By contrast, when we applied a significant amount of diffusion, $R_e = R_m$, we found that the growth rate for the $m = 1$ antisymmetric $(\tilde{\psi}_a, \tilde{\chi}_s)$ can be **increased** by diffusion, while the growth rate for the symmetric $(\tilde{\psi}_s, \tilde{\chi}_a)$ disturbances is always reduced. In consequence, the antisymmetric disturbances play a more important role in the instability than the symmetric disturbances when diffusion is present. Note that for the radial diffusive drag case, Dikpati *et al.* (2004), the diffusion always decreased the growth rate.

In figure 1 we show the growth rate $m\omega_i$ for $m = 1$ antisymmetric modes as a function of magnetic field strength a at zero diffusion for a variety of s_2 . These results are consistent with the diffusionless results of GF97, and show that indeed instability can occur for s_2 much less than 0.286 when magnetic field is present. In figure 2 we also show the growth rate as a function of a for various s_2 , but now weak diffusion is present, $R_e = R_m = 7000$. The growth rates are generally much faster than in figure 1, showing that diffusion is strongly destabilising. Even more remarkably, we have instability even for $s_2 = 0$, i.e. solid body rotation. This makes it clear that the source of the instability is the magnetic field. However, the diffusion is clearly playing a crucial role in this instability, because if $s_2 = 0$ in the diffusionless case, no instability occurs. The case $s_2 = 0$ was stable in both the Watson (1981) analysis and in GF97.

Figure 2 also shows that the $s_2 = 0.0$ up to $s_2 = 0.15$ curves have a different behaviour for $a < \approx 0.5$ than for $a > \approx 0.5$. For small values of a , lower differential rotation such as $s_2 = 0.0$ can give faster growth rates than higher differential rotation $s_2 = 0.09$. Here the differential rotation is interfering with instability rather than enhancing it. This is further evidence that the instability of this antisymmetric $m = 1$ mode is magnetically driven. However, when we exceed $a = 0.5$ we find that growth rates increase as the differential rotation is increased. So here the differential rotation is enhancing instability, adding to the instability of the magnetic field and leading to very large growth rates. So for the lower values of s_2 there is a critical value of $a \approx 0.5$, corresponding

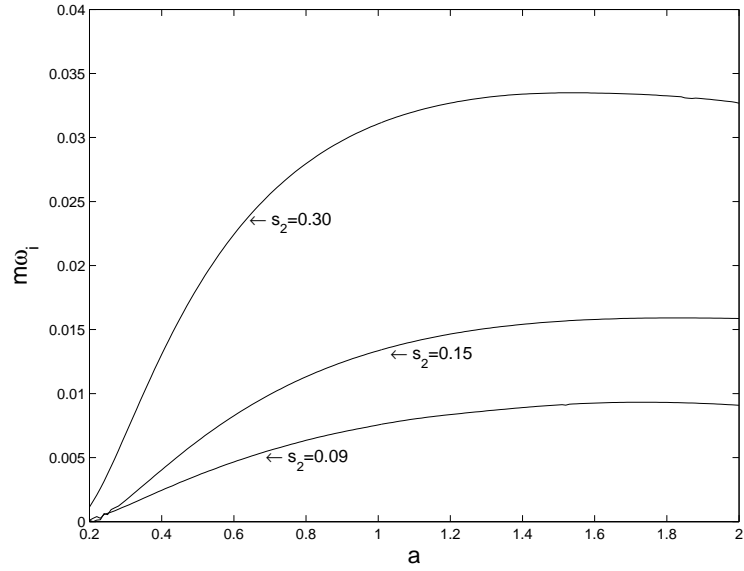


FIGURE 1. Growth rate $m\omega_i$ for $m = 1$ antisymmetric modes $(\tilde{\psi}_a, \tilde{\chi}_s)$ as function of toroidal field parameter a . The curves are for different differential rotation parameters s_2 . $R_e = R_m \rightarrow \infty$.

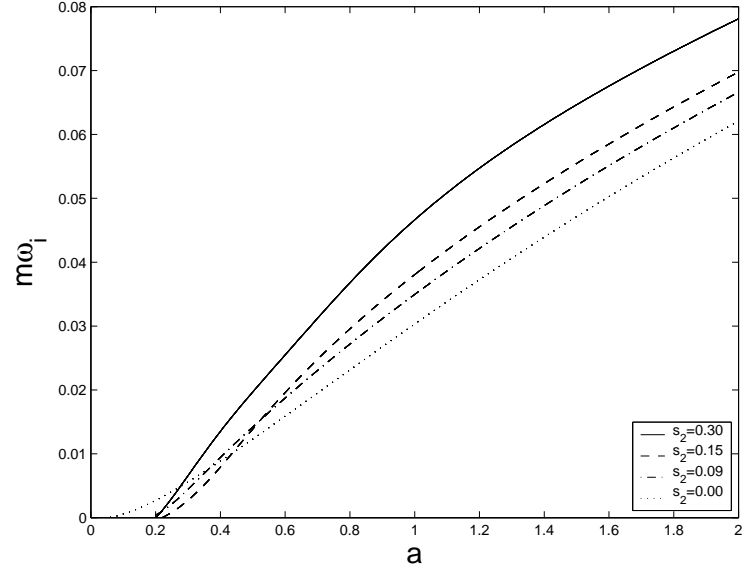


FIGURE 2. Growth rate $m\omega_i$ for $m = 1$ antisymmetric modes $(\tilde{\psi}_a, \tilde{\chi}_s)$ as function of toroidal field parameter a . The curves are for differential rotation parameters s_2 as indicated in the box. $R_e = R_m = 7000$.

to a peak field of 55,000G, below which differential rotation impedes instability and above which differential rotation enhances instability.

Figure 3 illustrates the growth rate for the same values of s_2 in figure 2, with Reynolds number decreased to 70. We increased the diffusion parameter to see if the growth rate, $m\omega_i$, starts to fall as a is increased. However, we found no turning point, indicating that increasing magnetic field

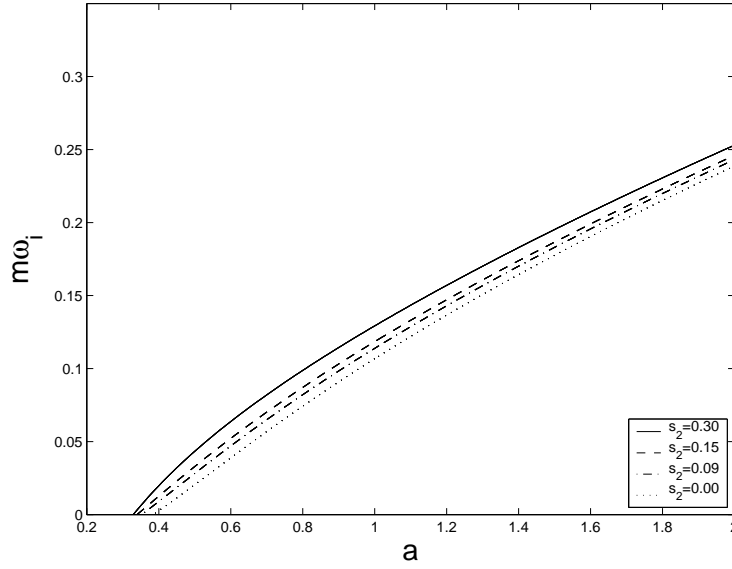


FIGURE 3. Growth rate $m\omega_i$ for $m = 1$ antisymmetric modes $(\tilde{\psi}_a, \tilde{\chi}_s)$ as function of toroidal field parameter a . The curves are for differential rotation parameters s_2 as indicated in the box. $R_e = R_m = 70$.

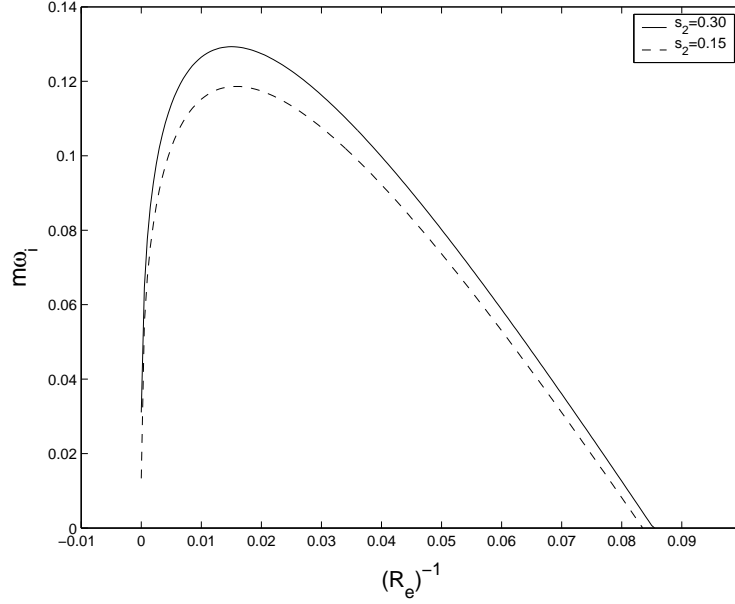


FIGURE 4. Growth rate $m\omega_i$ for $m = 1$ antisymmetric modes, (ψ_a, χ_s) , as a function of diffusion $(R_e = R_m)^{-1}$ for differential profiles $s_2=0.30$ and 0.15 . Toroidal field strength $a = 1$.

always makes the growth rate faster and this is again consistent with instability being magnetically driven. Interestingly, with this higher diffusion rate the growth rate is now much faster, and even field strengths just beyond critical have much faster growth rates than in the ideal GF97 case. In figure 4, we examine the growth rate as function of the diffusion parameter, fixing $a = 1.0$, and considering $s_2 = 0.3$ and $s_2 = 0.15$ for the $m = 1$ antisymmetric mode. We find there is a maximum

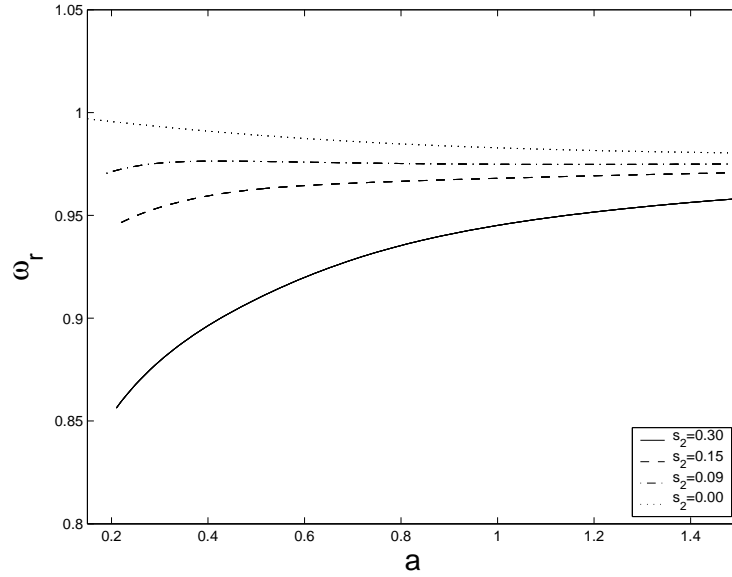


FIGURE 5. Phase velocity ω_r for $m = 1$ antisymmetric modes, $(\tilde{\psi}_a, \tilde{\chi}_s)$. For all a , the differential rotation parameter $s_2 = 0.30$ has the lowest phase velocity, $s_2 = 0.0$ the highest. $R_e = R_m = 7000$.

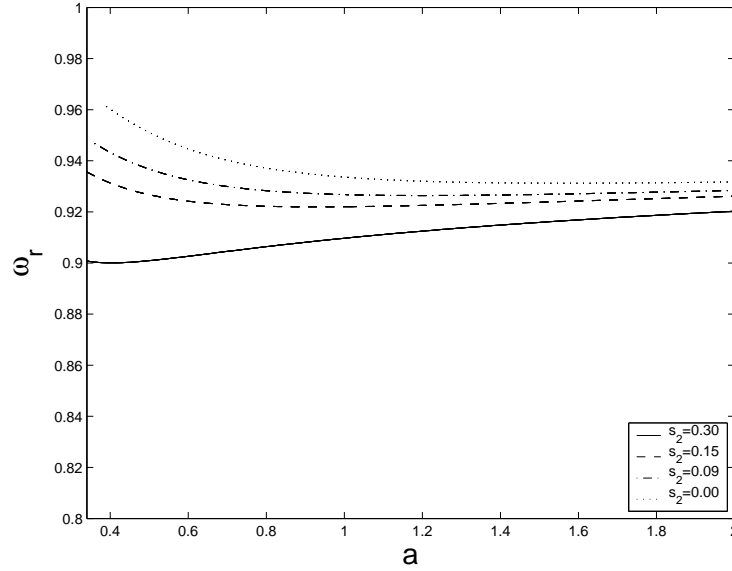


FIGURE 6. Phase velocity ω_r for $m = 1$ antisymmetric modes, $(\tilde{\psi}_a, \tilde{\chi}_s)$. For all a , the differential rotation parameter $s_2 = 0.30$ has the lowest phase velocity, $s_2 = 0.0$ the highest. $R_e = R_m = 70$.

growth rate $m\omega_i \approx 0.125$ when $R_e = R_m \approx 70$. If the diffusion is larger than this, the disturbance is damped out, but if the diffusion is small ($R_e = R_m \gg 70$) then the growth rate tends to its lower ideal MHD value. This again emphasises the importance of the diffusion in describing these instabilities. Since $R_e = 70$ corresponds to a rather high diffusion in the tachocline, we are almost certain to be in the regime where diffusion is strongly destabilising.

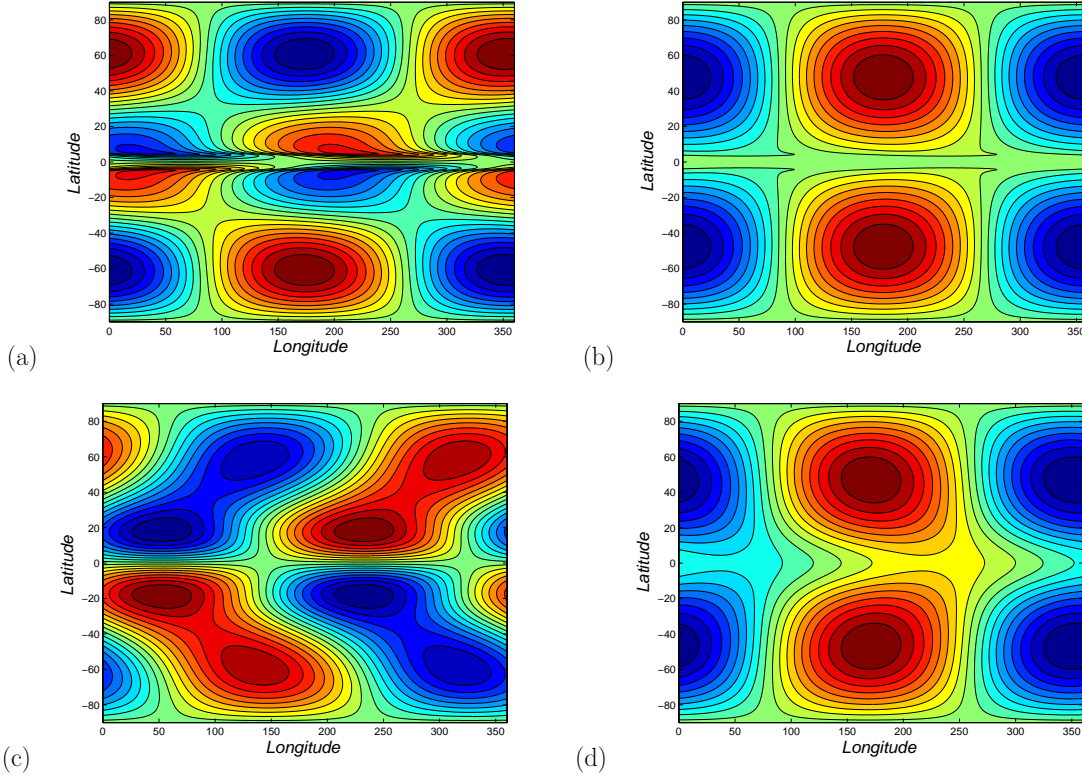


FIGURE 7. Contours of the eigenfunctions $\tilde{\psi}$ and $\tilde{\chi}$ as a function of longitude and latitude, with $s_2 = 0.15$ and $a = 0.5$. (a) Velocity streamfunction $\tilde{\psi}$ with no diffusion: (b) Magnetic field perturbations $\tilde{\chi}$ with no diffusion: (c) $\tilde{\psi}$ with $R_e = R_m = 700$: (d) $\tilde{\chi}$ with $R_e = R_m = 700$

Figures 5 and 6 show the phase velocities for the same cases as shown in figures 2 and 3 respectively. The phase speed is scaled with respect to the equatorial rotation rate. When $R_e = 7000$, figure 5, the phase velocities ω_r are almost identical with the ideal MHD case. In figure 5, for $s_2 = 0.30$, $s_2 = 0.15$, and $s_2 = 0.09$, ω_r starts to increase and converge to 0.955 as we increase the intensity of the toroidal field, a . However, for $s_2 = 0$, the frequency initially decreases and then converges to the same speed value as the other differential profiles as $a \rightarrow \infty$.

Now we consider the extreme case when $R_e \approx 70$, figure 6, where we see that for most cases the phase velocity decreases except for the strongest differential rotation case $s_2 = 0.30$ where ω_r increases with a . However, for all s_2 values $\omega_r \rightarrow 0.93$ as $a \rightarrow \infty$. This indicates that as we increase the field strength the phase velocity becomes almost constant for any value of s_2 and any amount of dissipation.

In figure 5 we see that for the solid body rotation case the phase velocity ω_r becomes close to unity as a is reduced. This means that the unstable waves have a slow phase velocity in the rotating frame. Furthermore, if $R_e = R_m$ is increased above 7000, the critical magnetic field strength a required for instability reduces, with $a_{crit} \sim O(R_m^{-1/2})$. This suggests that the joint limit $R_m \rightarrow \infty$, $a \rightarrow 0$ with $a^2 \sim R_m^{-1}$ is a useful limit to study. Our numerical results indicate that $\Omega - \omega_r \sim a^2$ in this limit, so that the first term in equation (9) and the viscous diffusion term on the R.H.S. of (9)

become negligible in this limit. $\tilde{\psi}$ scales with $a\tilde{\chi}$, so all three terms in equation (10) remain, and the system reduces to a second order ODE,

$$\left(a^2\mu + \frac{2i\Omega}{\mu m R_m}\right) \left(\frac{d}{d\mu}(1-\mu^2)\frac{d\tilde{\chi}}{d\mu} - \frac{m^2\tilde{\chi}}{1-\mu^2}\right) + 6\mu a^2\tilde{\chi} - \frac{2\Omega(\Omega-\omega)}{\mu}\tilde{\chi} = 0. \quad (18)$$

This equation has solutions regular at the poles with complex $\tilde{\chi}$ but real ω , corresponding to the neutrally stable modes at the stability boundary. Values of a greater than the critical value determined by (18) are unstable. This shows that it is the magnetic diffusion rather than the viscous diffusion which is important in this instability. Since the time-dependent term has disappeared from equation (9), which is the radial vorticity equation, the waves progress by evolving through a quasi-static equilibrium between the Lorentz force terms and the ‘beta’ effect term, the second on the L.H.S. of equation (9), which measures the change in radial vorticity as the ‘planetary’ vorticity due to the solid body rotation is advected to different latitudes. In dimensional terms, the phase speed of these waves is of order $B_0^2/\Omega_0 r_0^2 \mu_0 \rho$, which is the slow magnetic wave speed, sometimes called the MAC wave speed (Braginsky 1967, Fearn *et al.* 1988).

Since the $m = 1$ antisymmetric modes appear to be the most important modes in the presence of diffusion, we show only the eigenfunctions in these cases. Figures 7a and 7b are for the ideal MHD case, with $s_2 = 0.15$ and $a = 0.5$. Figure 7a shows the velocity streamfunction, which has a surprisingly complex structure. The flow is clockwise around the negative $\tilde{\psi}$ values, anticlockwise around the positive values. The jet flow near the equator is evident, and the $m = 1$ nature of the instability means that if the flow is eastward at one longitude, it is westward 180° further on in longitude. Since the flow therefore diverges in the latitudinal direction at one point and converges at the diametrically opposite point, toroidal magnetic field is opened up at one longitude, whilst being brought closer together at the opposite point. Cally *et al.* (2003) describe this as a ‘clamshell’ instability. The corresponding magnetic field perturbation, figure 7b, confirms this interpretation. At longitude 180° , for example, the perturbation adds to the positive reference state toroidal field B_ϕ in the northern hemisphere and also enlarges the negative reference state toroidal field in the southern hemisphere, so longitude 180° is a region in which the field intensifies due to the convergence of the latitudinal flow here. Conversely, near longitude 0° the perturbation weakens the basic state field.

Figures 7c and 7d are the corresponding figures in the presence of diffusion. Comparing with the ideal MHD case, it can be seen that some streamline reconnection has taken place, and now there are sloping circulation cells above and below the equator. The basic ‘clamshell’ nature of the instability is still there, however, as can be seen from figure 7d.

The case of the $m = 1$ symmetric mode is less interesting, because here diffusion always appears to be stabilising. GF97 found that for $s_2 = 0.30$ the highest growth rate occurred when $a \approx 0.17$. In figure 8 we show the effect of diffusion on the growth rate for this $s_2 = 0.30$, $a = 0.17$ case, and we see the instability is damped completely when the Reynolds number is reduced below around 1,000. For lower values of s_2 this occurs at even higher Reynolds numbers, and increasing the magnetic field strength does not alter the situation much either. The symmetric $m = 1$ mode is only important at low values of $a \approx 0.1$ where the symmetric mode can be unstable where the antisymmetric mode is still stable. However, even then, only small amounts of diffusion are needed to eliminate this symmetric mode instability.

GF97 also stated in their report (1997) that ‘the instability appears to occur only for longitudinal wave number 1’. Actually, we found a small region of the parameter space where ideal MHD unstable $m = 2$ antisymmetric modes exist. As with the $m = 1$ antisymmetric modes diffusion can enhance instability, so the region where unstable modes $m = 2$ occur is enlarged as shown in figure 9. The only differential rotation profile for which we could obtain convincing evidence of ideal MHD instability was when $s_2 = 0.30$. Below $a = 0.25$ very large truncations are needed to

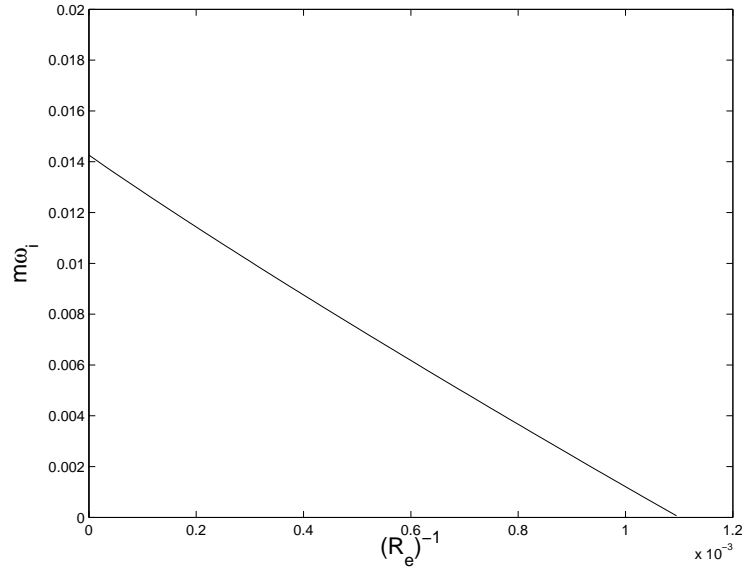


FIGURE 8. Growth rate for $m = 1$ symmetric mode, $(\tilde{\psi}_s, \tilde{\chi}_a)$, for $s_2 = 0.30$, toroidal field $a = 0.17$ as a function of diffusion $(R_e = R_m)^{-1}$.

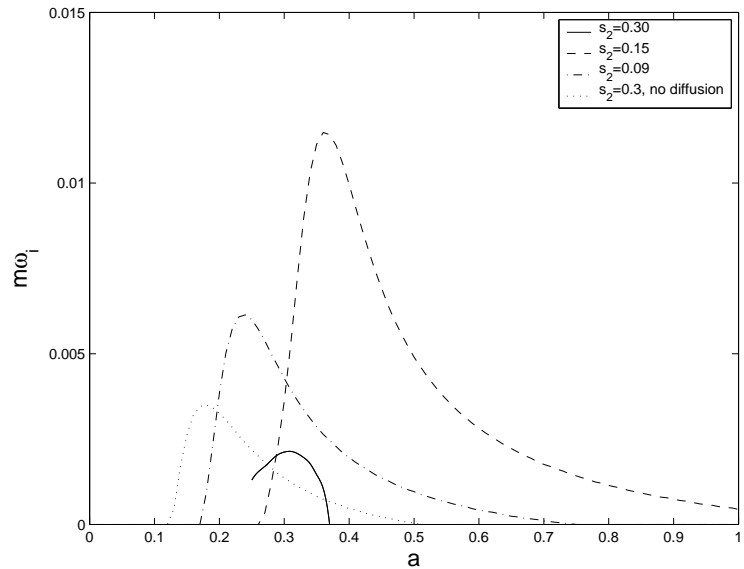


FIGURE 9. Growth rate for $m = 2$ antisymmetric modes, $(\tilde{\psi}_a, \tilde{\chi}_s)$ as a function of toroidal field strength a . The cases for $s_2 = 0.30, 0.15$ and 0.09 with diffusion corresponding to $R_e = R_m = 7000$ are shown, together with the case $s_2 = 0.30$ with no diffusion.

resolve the eigenfunctions even for this case, so we were not able to go below $a = 0.25$. Generally, convergence is much better in the diffusive cases than in the ideal MHD cases. At Reynolds numbers approaching $R_e = 7000$, we obtained $m = 2$ instability for a range of s_2 values, also shown in figure 9. We have selected some of the same profiles as we did in the $m = 1$ antisymmetric case, figure 2. Interestingly, the shape of the curves in the $m = 2$ figure 9 case are quite different from the equivalent $m = 1$ antisymmetric modes shown in figure 2. For $m = 2$ modes there is a maximum

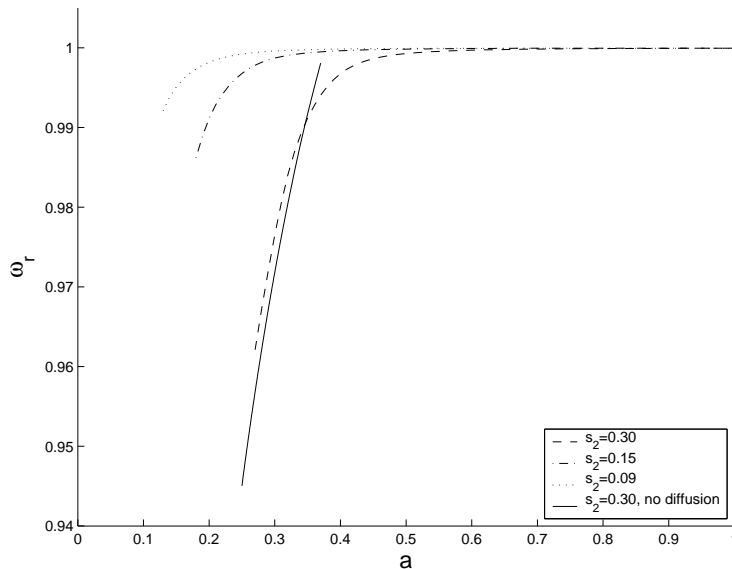


FIGURE 10. Phase velocity for $m = 2$ antisymmetric modes, $(\tilde{\psi}_a, \tilde{\chi}_s)$ as a function of toroidal field strength a . The cases for $s_2 = 0.30$, 0.15 and 0.09 with diffusion corresponding to $R_e = R_m = 7000$ are shown, together with the case $s_2 = 0.30$ with no diffusion.

growth rate as a is varied, and the modes restabilise at large magnetic field strengths, whereas for the $m = 1$ mode the growth rate increases without limit as the field is increased. As we reduce the Reynolds number below 7000, all of these $m = 2$ antisymmetric modes become stable. The corresponding phase velocity diagrams are shown in figure 10, which can be compared with the $m = 1$ phase velocities in figure 6. Again, the limiting behaviour at large a is somewhat different in the two cases, because in the $m = 1$ case the phase velocity is significantly less than 1, but in the $m = 2$ case the phase velocity approaches 1, which means that the critical layer at which phase and fluid velocities are equal approaches the equator.

5. Conclusions

The two-dimensional diffusive instability model considered here behaves rather differently from the radial diffusion model of Dikpati *et al.* (2004). The assumption made here is that diffusion along surfaces of constant r dominates any diffusion in the radial direction, which is valid in the limit in which the stratification is strong enough so that any radial eddy motion is suppressed. This is the opposite limit of the case where radial diffusion dominates, and in reality some mixture of the two is probably more appropriate in the tachocline, particularly close to the convection zone where the stable stratification is not so strong.

The main difference between the two diffusion models is that the radial diffusion model was found to be stabilising, whereas for two-dimensional diffusion the important $m = 1$ antisymmetric mode is strongly destabilised, even for fairly weak diffusion. Since in this model instability can occur even for the case of solid body rotation, it is clear that this instability is a magnetic instability and not a joint magnetic/rotational (magneto-rotational) instability as in the ideal MHD case. This has important consequences for the behaviour of the instability both at large and small magnetic field strengths. At large field strengths, the growth rates can grow without limit as the magnetic field increases, and at small field strengths differential rotation may impede rather than aid instability.

This new instability appears to have the $m = 1$ antisymmetric mode as the dominant case. Symmetric modes are stabilised by two-dimensional diffusion (as they are by radial diffusion) and

have a limited range of importance, though they can still dominate for weak field strengths and very low diffusion. Unstable $m = 2$ antisymmetric modes can also appear, though growth rates are significantly less than for the $m = 1$ modes. We have not explored $m = 3$ and beyond.

The numerical method adopted was found to give satisfactory results, though the ideal MHD case does sometimes require very high truncations, particularly near marginal stability, so calculations here can be very CPU-intensive. The diffusive equations are much better behaved, so that although the equations are of higher differential order they are much easier to solve numerically. Even small amounts of diffusion allow the the truncation level N to be significantly reduced, thus speeding up the computations substantially.

As noted by Dikpati *et al.* (2004), there is not much direct observational evidence for the ‘clamshell’ type of $m = 1$ antisymmetric instability of the type found here. However, since the instability occurs in the region shielded by the whole solar convection zone this may not be too surprising. The dynamics of the tachocline is a significant issue in solar physics, and further studies, particularly nonlinear studies, may help to unlock some of its secrets.

Acknowledgements

We are grateful to Peter Gilman and an anonymous referee for helpful comments.

References

- Abramowitz, M. and Stegun, I.A., *Handbook of mathematical functions*, 1970, Dover.
- Braginsky, S.I. Magnetic waves in the Earth’s core. *Geomagn. & Aeron.*, 1967, **7**, 851–859.
- Brown, T.M., Christensen-Dalsgaard, J., Dziembowski, W.A., Goode, P., Gough, D.O. and Morrow, C.A., Inferring the Sun’s internal angular velocity from observed p-mode frequency splittings. *Astrophys. J.*, 1989, **343**, 526–546.
- Cally, P.S., Three dimensional magneto–shear instability in the solar tachocline. *Mon. Not. R. Astr. Soc.*, 2003, **339**, 957–972.
- Cally, P.S., Dikpati, M. and Gilman, P.A., Clamshell and tipping instabilities in a two-dimensional magnetohydrodynamic tachocline. *Astrophys. J.*, 2003, **582**, 1190–1205.
- Chan, K.H., Liao, X., Zhang, K. and Jones, C.A., Non-axisymmetric spherical interface dynamos. *Astron. Astrophys.*, 2004, **423**, L37–40.
- Charbonneau, P. and MacGregor, K.B., Solar interface dynamos. II. Linear, kinematic model in spherical geometry. *Astrophys. J.*, 1997, **486**, 502–520.
- Charbonneau, P., Christensen-Dalsgaard, J., Henning, R., Larsen, R.M., Schou, J., Thompson, M.J., and Tomczyk, S., Helioseismic constraints on the structure of the solar tachocline. *Astrophys. J.*, 1999, **527**, 446–460.
- Charbonneau, P., Dikpati, M. and Gilman, P.A., Stability of the solar latitudinal differential rotation inferred from helioseismic data. *Astrophys. J.*, 1999, **526**, 523–537.
- Dikpati, M., Cally, P.S. and Gilman, P.A., Linear analysis and nonlinear evolution of two-dimensional global magnetohydrodynamic instabilities in a diffusive tachocline. *Astrophys. J.*, 2004, **610**, 597–615.
- Durney, B., The energy lost by differential rotation in the generation of the solar toroidal magnetic field. *Solar Physics.*, 2000, **197**, 215–226.
- Fearn, D.R., Roberts, P.H. and Soward, A.M., Convection, stability and the dynamo, in *Energy, Stability and Convection* (eds G.P.Galdi and B. Straughan). Longmans, 1988, pp 60–324.
- Forgács-Dajka, E. and Petrovay, K., Tachocline confinement by an oscillatory magnetic field. *Solar Physics.*, 2001, **203**, 195–210.
- Gilman, P.A. and Fox, P., Joint instability of the latitudinal differential rotation and toroidal magnetic fields below the solar convection zone. *Astrophys. J.*, 1997, **484**, 439–454.

- Guenther, D.B., DeMarque, P., Kim, Y.C. and Pinsonneault, M.H., Standard solar model. *Astrophys. J.*, 1992, **387**, 372-393.
- Kosovichev, A.G., Helioseismic constraints on the gradient of angular velocity at the base of the solar convection zone. *Astrophys. J.*, 1996, **469**, L61-L64.
- Roberts, P.H. and Soward, A.M., Dynamo theory *Ann. Rev. Fluid Mech.*, 1992, **24**, 459-512.
- Rüdiger, G., *Differential rotation and stellar convection*, 1989, Gordon and Breach.
- Schou, J. and 23 others, Helioseismic studies of differential rotation in the solar envelope by the solar oscillations investigation using the Michelson Doppler Imager. *Astrophys. J.*, 1998, **505**, 390-417.
- Sharif, B.W., Rotational and magnetic instability in the diffusive tachocline. *Ph.D. Thesis, University of Exeter*, 2005.
- Spiegel, E. and Zahn, J-P., The solar tachocline. *Astron. Astrophys.*, 1992, **265**, 106-114.
- Watson, M., Shear instability of differential rotation in stars. *Geophys. Astrophys. Fluid Dyn.*, 1981, **16**, 285-298.
- Zhang K, Chan, K.H., Zou, J., Liao, X., and Schubert, G., A Three-Dimensional Spherical Non-linear Interface Dynamo. *Astrophys. J.*, 2003, **596**, 663-679.

Appendix A

We need to derive the matrix eigenvalue problem for ω from equations (16) and (17). The matrices have a block structure which depends on whether the equatorially symmetric or antisymmetric modes are sought. For the symmetric case the block structure is

$$\begin{bmatrix} A & B \\ \hline C & D \end{bmatrix} \begin{bmatrix} a_m \\ \vdots \\ a_{m+2N} \\ b_{m+1} \\ \vdots \\ b_{m+2N+1} \end{bmatrix} = -\omega \begin{bmatrix} a_m \\ \vdots \\ a_{m+2N} \\ b_{m+1} \\ \vdots \\ b_{m+2N+1} \end{bmatrix} \quad (\text{A1})$$

and for the antisymmetric modes the block structure is similar, except that the vectors

$$(a_m, a_{m+2} \dots a_{m+2N}, b_{m+1}, b_{m+3} \dots b_{m+2N+1}) \quad (\text{A2})$$

are replaced by the vectors

$$(a_{m+1}, a_{m+3} \dots a_{m+2N+1}, b_m, b_{m+2} \dots b_{m+2N}). \quad (\text{A3})$$

In both cases the whole matrix is of order $(2N+2) \times (2N+2)$. The blocks A and D are tridiagonal matrices in both cases, but in the symmetric case B has only a leading diagonal and one subdiagonal, while C has only a leading diagonal and one superdiagonal. In the antisymmetric case, B has a leading diagonal and one superdiagonal, while C has a leading diagonal and one subdiagonal.

When the expression $\Omega = 1 - s_2 \mu^2$ is substituted into (16) and (17), terms involving μP_n^m and $\mu^2 P_n^m$ appear. These are eliminated using the recurrence relations for associated Legendre polynomials

$$\mu P_n^m = \frac{(n-m+1)}{2n+1} P_{n+1}^m + \frac{(m+n)}{2n+1} P_{n-1}^m, \quad (\text{A4})$$

and

$$\mu^2 P_n^m = \frac{(n-m+1)(n-m+2)}{(2n+1)(2n+3)} P_{n+2}^m + \frac{(2n^2+2n-1-2m^2)}{(2n-1)(2n+3)} P_n^m + \frac{(n+m)(n+m-1)}{(2n+1)(2n-1)} P_{n-2}^m, \quad (\text{A5})$$

the second of which follows from the first, which is in Abramowitz and Stegun (1970). The matrices we need are then found by equating the coefficients of P_n^m to zero in both (16) and (17). We get from the vorticity equation (16)

$$R_n a_{n-2} + S_n a_n + T_n a_{n+2} + L_n b_{n-1} + M_n b_{n+1} = -\omega a_n, \quad (\text{A6})$$

where $n = m + 2i$, $i = 0, N$ and $R_m = L_m = T_{m+2N} = 0$ in the symmetric case, and $n = m + 2i + 1$, $i = 0, N$, $R_{m+1} = T_{m+2N+1} = M_{m+2N+1} = 0$ in the antisymmetric case. The coefficients are

$$R_n = \frac{s_2(n-m-1)(n-m)[(n-2)(n-1)-12]}{(2n-3)(2n-1)n(n+1)},$$

$$S_n = -1 - (imR_e)^{-1}n(n+1) + \frac{2(1+s_2)}{n(n+1)} + \frac{s_2[2n(n+1)-1-2m^2][n(n+1)-12]}{(2n-1)(2n+3)n(n+1)},$$

$$T_n = \frac{s_2(n+m+1)(n+m+2)[(n+2)(n+3)-12]}{(2n+3)(2n+5)n(n+1)},$$

$$L_n = \frac{a[n(n-1)-6](n-m)}{(2n-1)n(n+1)}, \quad \text{and} \quad M_n = \frac{a[(n+1)(n+2)-6](n+m+1)}{n(n+1)(2n+3)}.$$

The blocks A and B for the symmetric case are therefore of the form

$$A = \begin{bmatrix} S_m & T_m & 0 & \dots \\ R_{m+2} & S_{m+2} & T_{m+2} & \dots \\ \dots & \dots & \dots & \dots \\ \dots & 0 & R_{m+2N} & S_{m+2N} \end{bmatrix}, \quad B = \begin{bmatrix} M_m & 0 & \dots & \dots \\ L_{m+2} & M_{m+2} & 0 & \dots \\ \dots & \dots & \dots & \dots \\ \dots & \dots & L_{m+2N} & M_{m+2N} \end{bmatrix},$$

while in the antisymmetric case

$$A = \begin{bmatrix} S_{m+1} & T_{m+1} & 0 & \dots \\ R_{m+3} & S_{m+3} & T_{m+3} & \dots \\ \dots & \dots & \dots & \dots \\ \dots & 0 & R_{m+2N+1} & S_{m+2N+1} \end{bmatrix}, \quad B = \begin{bmatrix} L_{m+1} & M_{m+1} & 0 & \dots \\ 0 & L_{m+3} & M_{m+3} & \dots \\ \dots & \dots & \dots & \dots \\ \dots & \dots & 0 & L_{m+2N+1} \end{bmatrix}.$$

Note that if the toriodal field is set to be zero, $a = 0$, then we have

$$R_n a_{n-2} + S_n a_n + T_n a_{n+2} = -\omega a_n \quad (\text{A7})$$

which is the form of Watson's three term recurrence relation, see Watson (1981).

Similarly, by substituting the expressions for μP_n^m and $\mu^2 P_n^m$ into the magnetic field equation(17), we obtain

$$F_n a_{n-1} + G_n a_{n+1} + A_n b_{n-2} + B_n b_n + C_n b_{n+2} = -\omega b_n, \quad (\text{A8})$$

where for the symmetric case $n = m + 2i + 1$, $i = 0, N$, and $A_{m+1} = C_{m+2N+1} = G_{m+2N+1} = 0$ and for the antisymmetric case $n = m + 2i$, $i = 0, N$, and $A_m = F_m = C_{m+2N} = 0$. The coefficients are given by

$$F_n = \frac{a(n-m)}{(2n-1)}, \quad G_n = \frac{a(n+m+1)}{(2n+3)},$$

$$A_n = \frac{s_2(n-m-1)(n-m)}{(2n-3)(2n-1)}, \quad B_n = -1 - (imR_m)^{-1}n(n+1) + \frac{s_2[2n(n+1)-1-2m^2]}{(2n-1)(2n+3)},$$

and

$$C_n = \frac{s_2(n+m+1)(n+m+2)}{(2n+3)(2n+5)}.$$

The structure of the blocks C and D are in the symmetric case

$$C = \begin{bmatrix} F_{m+1} & G_{m+1} & 0 & \dots \\ 0 & F_{m+3} & G_{m+3} & \dots \\ \dots & \dots & \dots & \dots \\ \dots & \dots & 0 & F_{m+2N+1} \end{bmatrix}, \quad D = \begin{bmatrix} B_{m+1} & C_{m+1} & 0 & \dots \\ A_{m+3} & B_{m+3} & C_{m+3} & \dots \\ \dots & \dots & \dots & \dots \\ \dots & 0 & A_{m+2N+1} & B_{m+2N+1} \end{bmatrix},$$

while in the antisymmetric case they are

$$C = \begin{bmatrix} G_m & 0 & \dots & \dots \\ F_{m+2} & G_{m+2} & 0 & \dots \\ \dots & \dots & \dots & \dots \\ \dots & \dots & 0 & G_{m+2N} \end{bmatrix}, \quad D = \begin{bmatrix} B_m & C_m & 0 & \dots \\ A_{m+2} & B_{m+2} & C_{m+2} & \dots \\ \dots & \dots & \dots & \dots \\ \dots & 0 & A_{m+2N} & B_{m+2N} \end{bmatrix}.$$

For both symmetries we have a square $(2N + 2) \times (2N + 2)$ matrix eigenvalue problem which can be solved using standard numerical linear algebra software.